

Low Energy Wireless Body-Area Networks for Fetal ECG Telemonitoring via the Framework of Block Sparse Bayesian Learning

Zhilin Zhang, *Student Member, IEEE*, Tzyy-Ping Jung, *Senior Member, IEEE*
Scott Makeig, *Member, IEEE*, Bhaskar D. Rao, *Fellow, IEEE*

Abstract—Fetal ECG (FECG) telemonitoring is an important branch in telemedicine. The design of a telemonitoring system via a wireless body-area network with low energy consumption for ambulatory use is highly desirable. As an emerging technique, compressed sensing (CS) shows great promise in compressing/reconstructing data with low energy consumption. However, due to some specific characteristics of raw FECG recordings such as non-sparsity and strong noise contamination, current CS algorithms generally fail for this application.

This work proposes to use the Block Sparse Bayesian Learning (BSBL) framework to compress/reconstruct non-sparse raw FECG recordings. Experimental results show that the framework can reconstruct the raw recordings with high quality. Especially, the reconstruction does not destroy the interdependence relation among the multichannel recordings, ensuring independent component analysis (ICA) decomposition of the reconstructed recordings has high fidelity. Thus, the extracted FECGs using ICA from the reconstructed recordings have little distortion, satisfying requirements of clinical applications. Furthermore, the framework allows the use of a sparse binary sensing matrix with much fewer non-zero entries to compress recordings. Particularly, each column of the sensing matrix can contain only *two* non-zero entries, implying the framework has almost achieved the lowest energy consumption in compression.

Index Terms—Fetal ECG (FECG), Telemonitoring, Compressed Sensing (CS), Block Sparse Bayesian Learning (BSBL), Wireless Body-Area Network (WBAN), Telemedicine, Sparsity, Independent Component Analysis (ICA)

I. INTRODUCTION

Noninvasive monitoring of fetal electrocardiogram (FECG) is an important approach to monitor the health of fetuses. The characteristic parameters of an FECG, such as heart beat rates, morphology, and dynamic behaviors, can be used for diagnosis of fetal development and disease. Among these parameters, the heart beat rate is the main index of fetal assessment for high-risk pregnancies [1]. For example, abnormal patterns (decelerations, loss of high-frequency variability, and pseudo-sinusoidal) of fetal heart beat rates are generally indicative of fetal asphyxia [2].

The work was supported by NSF grants CCF-0830612, CCF-1144258 and DGE-0333451, and was in part supported by Army Research Lab, Army Research Office, Office of Naval Research and DARPA.

Z.Zhang and B.D.Rao are with the Department of Electrical and Computer Engineering, University of California, San Diego, La Jolla, CA 92093-0407, USA. Email: {z4zhang, brao}@ucsd.edu

T.-P. Jung and S. Makeig are with the Swartz Center for Computational Neuroscience, University of California, San Diego, La Jolla, CA 92093-0559, USA. Email: {jung, scott}@scn.ucsd.edu

However, to noninvasively obtain clean FECGs from maternal abdominal recordings is not an easy problem, since FECGs are very weak, and are often embedded in strong noise and interference, such as maternal ECGs (MECGs), instrumental noise, and artifacts caused by muscles. Further, the gestational age and the position of fetuses also affect the strength of FECGs. Up to now various signal processing and machine learning methods have been proposed to obtain FECGs, such as adaptive filtering [3], wavelet analysis [4], and blind source separation (BSS)/independent component analysis (ICA) [5]. For example, the problem of extracting clean FECGs from raw FECG recordings can be well modeled as an instantaneous ICA mixture model. In this model, the raw recordings are viewed as the linear mixture of a number of independent (or uncorrelated) sources including FECG components, MECG components, and various noise components [5]. Interested readers can refer to [2], [4], [6] for good surveys on these techniques.

Traditionally, pregnant women are required to frequently visit hospitals to get resting FECG monitoring. Now, the trend and desire is to allow pregnant women to receive ambulatory monitoring of FECG. For example, pregnant women can stay at home where FECGs can be collected through wireless telemonitoring. In such a telemonitoring system, a wireless body-area network (WBAN) [7] integrates a number of sensors attached on a patient's skin, and uses ultra-low-power short-haul radios (e.g., Bluetooth Low End Extension Radio) in conjunction with nearby smart-phones or handheld devices to communicate via the Internet with the health care provider in a remote terminal. Telemonitoring is a convenient way for patients to avoid frequent hospital visits and save lots of time and medical expenses.

Among many constraints in WBAN-based telemonitoring systems [8], the energy constraint is a primary design constraint [9] since a WBAN is often battery-operated. It is necessary to reduce energy consumption as much as possible. This has to be done in a constrained environment. One constraint is that on-sensor computation should be minimum. Another constraint is that data should be compressed before transmission (the compressed data will be used to reconstruct the original data in remote terminals). Unfortunately, most conventional data compression techniques such as wavelet-based algorithms dissipate lots of energy [10]. Therefore, new compression techniques are needed urgently.

Compressed sensing (CS) [11], [12], an emerging signal

processing technique, is a promising tool to cater to the two constraints. It uses a simple linear transform (i.e., a sensing matrix) to compress a signal, and then reconstructs it by exploiting its sparsity. The sparsity refers to the characteristics that most entries of the signal are zero. When CS is used in WBAN-based telemonitoring systems, the compression stage is completed on data acquisition module before transmission, while the reconstruction stage is completed on workstations/computers at remote receiving terminals. Based on a real-time ECG telemonitoring system, Mamaghanian et al. [10] showed that when using a sparse binary matrix as the sensing matrix, CS can greatly extend sensor lifetime and reduce energy consumption while achieving competitive compression ratio, compared to a wavelet-based compression method. They also pointed out that when the data collection and the compression are implemented together by analog devices before analog-to-digital converter (ADC), the energy consumption can be further reduced.

Although CS has achieved some successes in adult ECG telemonitoring [10], [13], [14], it encounters difficulties in FECG telemonitoring. These difficulties essentially come from the conflict between more strict energy constraint in FECG telemonitoring systems and non-sparsity of raw FECG recordings.

The energy constraint is more strict in FECG telemonitoring systems due to the large number of sensors deployed. Generally, the number of sensors to receive raw FECG recordings ranges from 8 to 16, and sometimes extra sensors are needed to record maternal physiological signals (e.g., blood pressure, MECCG, and temperature). The large number of sensors indicates large energy dissipated in on-sensor computation. Given limited energy, this requires the systems to perform as little on-sensor computation as possible. For example, filtering before data compression may be prohibited. For CS algorithms, this means that they are required to directly compress raw FECG recordings with none or minimum pre-processing.

However, raw FECG recordings are non-sparse, which seriously deteriorates reconstruction quality of CS algorithms. Raw FECG recordings differ from adult ECG recordings in that they are unavoidably contaminated by a number of strong noise and interference, as discussed previously. Most CS algorithms have difficulty in directly reconstructing such non-sparse signals. Although some strategies have been proposed to deal with non-sparse signals, they are not helpful to our application.

This study proposes to use the Block Sparse Bayesian Learning (BSBL) framework [15], [16] to address these challenges. The BSBL framework, as a new framework solving the CS problems, has some advantages over conventional CS frameworks. It provides large flexibility to exploit spatial [17], temporal [16], and dynamic structure [18] of signals. Algorithms derived using this framework have superior performance compared to most existing CS algorithms [19]. Here, we present two interesting properties of the BSBL framework. One is its ability to reconstruct non-sparse signals with high quality. The other is its ability to exploit unknown structure of signals for better reconstruction quality. These two properties make the BSBL framework successful in wireless FECG

telemonitoring.

The rest of the paper is organized as follows. Section II introduces basic CS models and the BSBL framework. Section III shows experiment results on two typical FECG datasets. Section IV discusses some issues related to the BSBL framework and our experiments. Discussions and conclusions are given in the last two sections.

II. COMPRESSED SENSING (CS) AND BLOCK SPARSE BAYESIAN LEARNING (BSBL)

As in the ‘digital CS’ paradigm in [10], we assume signals have passed through the analog-to-digital converter (ADC).

A. Compressed Sensing and Associated Models

Compressed sensing (CS) is a new signal compression paradigm which relies on the sparsity of signals to compress and reconstruct. The *basic noisy model* can be expressed as

$$\mathbf{y} = \Phi \mathbf{x} + \mathbf{v}, \quad (1)$$

where $\mathbf{x} \in \mathbb{R}^{N \times 1}$ is the signal to compress/reconstruct with length N . $\Phi \in \mathbb{R}^{M \times N}$ ($M \ll N$) is a designed sensing matrix which linearly compresses \mathbf{x} . Any M columns of Φ are linearly independent. \mathbf{v} is a noise vector modeling errors incurred during this compression procedure or noise in the CS system. In our application \mathbf{x} is a segment from a raw FECG recording, and \mathbf{y} is the compressed data which will be transmitted via a WBAN to a remote terminal.

In a remote terminal, using the designed sensing matrix Φ , a CS algorithm reconstructs \mathbf{x} from the compressed data \mathbf{y} . Note that reconstructing \mathbf{x} is an underdetermined inverse problem. By exploiting the sparsity of \mathbf{x} it is possible to recover it with small errors in the presence of noise [12].

In many applications the signal \mathbf{x} is not sparse, but sparse in some transformed domains such as the wavelet domain. This means, \mathbf{x} can be expressed as $\mathbf{x} = \Psi \boldsymbol{\theta}$, where $\Psi \in \mathbb{R}^{N \times N}$ is an orthonormal basis matrix of a transformed domain and $\boldsymbol{\theta}$ is the representation coefficient vector which is sparse. Thus the basic noisy model (1) becomes

$$\mathbf{y} = \Phi \Psi \boldsymbol{\theta} + \mathbf{v} = \Omega \boldsymbol{\theta} + \mathbf{v}, \quad (2)$$

where $\Omega \triangleq \Phi \Psi$. Since $\boldsymbol{\theta}$ is sparse, a CS algorithm can first reconstruct $\boldsymbol{\theta}$ using \mathbf{y} and Ω , and then reconstruct \mathbf{x} by $\mathbf{x} = \Psi \boldsymbol{\theta}$. This method is useful for some kinds of signals. But as shown in our experiments later, this method still cannot help existing CS algorithms to reconstruct raw FECG recordings.

Sometimes the noise vector \mathbf{v} can be ignored, but the signal \mathbf{x} itself contains noise (called ‘*signal noise*’). That is, $\mathbf{x} = \mathbf{u} + \mathbf{n}$, where \mathbf{u} is the clean signal and \mathbf{n} is the signal noise. Thus the model (1) becomes

$$\mathbf{y} = \Phi \mathbf{x} = \Phi (\mathbf{u} + \mathbf{n}) = \Phi \mathbf{u} + \Phi \mathbf{n} = \Phi \mathbf{u} + \mathbf{w}, \quad (3)$$

where $\mathbf{w} \triangleq \Phi \mathbf{n}$ is a new noise vector. This model is also called a ‘*noise-folding model*’, and can be viewed as a basic noisy CS model [20].

Most natural signals have rich structure. A widely existing structure in natural signals is block structure [21]. A sparse

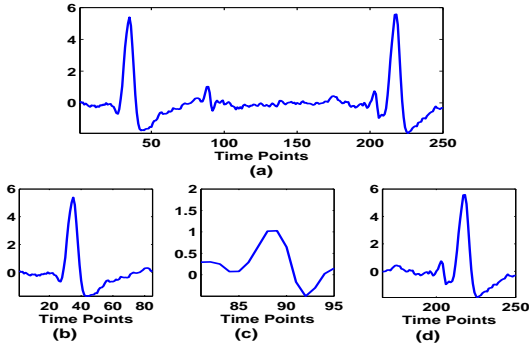


Fig. 1. Close-up of the second channel recording in the DaISy Dataset in Fig.4. (a) A segment of the first 250 time points of the recording. (b) A sub-segment containing a QRS complex of the MEGC. (c) A sub-segment containing a QRS complex of the FECG. (d) A sub-segment showing a QRS complex of the FECG contaminated by a QRS complex of the MEGC.

signal with this structure can be viewed as a concatenation of a number of blocks, i.e

$$\mathbf{x} = \underbrace{[x_1, \dots, x_{h_1}]^T}_{\mathbf{x}_1^T}, \dots, \underbrace{[x_{h_{g-1}+1}, \dots, x_{h_g}]^T}_{\mathbf{x}_g^T} \quad (4)$$

where $\mathbf{x}_i \in \mathbb{R}^{h_i \times 1}$, and $h_i (i = 1, \dots, g)$ are not necessarily identical. Among these blocks, only few blocks are non-zero. A signal with this block structure is called a *block-sparse signal*, and the model (1) with the block partition (4) is called a *block-sparse model*. It is known that exploiting such block structure can further improve reconstruction performance [15], [22], [21].

A raw FECG recording can be roughly viewed as a block-sparse signal contaminated by signal noise. Figure 1 (a) plots a segment of a raw FECG recording. In this segment the parts from 20 to 60, from 85 to 95, and from 200 to 250 time points can be viewed as three significant non-zero blocks. Other parts can be viewed as concatenations of zero blocks. And the whole segment can be viewed as contaminated by signal noise. Note that although the block partition can be roughly determined by observing the raw recording, in practical FECG telemonitoring the block partition is unknown. Hence, a raw FECG recording can be modeled as a block-sparse model with unknown block partition and unknown signal noise in a noiseless environment.

Reconstructing \mathbf{x} while exploiting its unknown block partition is very difficult. Up to now only several CS algorithms have been proposed for this purpose [23], [24], [25]. Recently we proposed the framework of Block Sparse Bayesian Learning (BSBL) [15], [16], and derived a family of algorithms [15]. Their abilities to reconstruct less-sparse signals and structured signals with unknown block partition endow them with superior performance to existing algorithms. In the following we will briefly introduce it. Interested readers can refer to [15], [16], [26] for details.

B. Block Sparse Bayesian Learning (BSBL)

For a block-sparse signal \mathbf{x} of the form (4), the BSBL framework models each block $\mathbf{x}_i \in \mathbb{R}^{d_i \times 1}$ as a parameterized

multivariate Gaussian distribution:

$$p(\mathbf{x}_i; \gamma_i, \mathbf{B}_i) \sim \mathcal{N}(\mathbf{0}, \gamma_i \mathbf{B}_i), \quad i = 1, \dots, g \quad (5)$$

where γ_i is a nonnegative parameter controlling the block-sparsity of \mathbf{x} . When $\gamma_i = 0$, the corresponding i -th block, i.e., \mathbf{x}_i , becomes a zero block. $\mathbf{B}_i \in \mathbb{R}^{d_i \times d_i}$ is a positive definite matrix capturing the correlation structure of the i -th block. With the assumption that blocks are mutually uncorrelated, according to (5), the prior of \mathbf{x} is $p(\mathbf{x}) \sim \mathcal{N}(\mathbf{0}, \mathbf{\Sigma}_0)$, where $\mathbf{\Sigma}_0$ is a block-diagonal matrix with each principal block given by $\gamma_i \mathbf{B}_i$. The noise vector is assumed to satisfy a multivariate Gaussian distribution, namely $p(\mathbf{v}) \sim \mathcal{N}(\mathbf{0}, \lambda \mathbf{I})$, where λ is a positive scalar and \mathbf{I} is the identity matrix.

Thus, the estimate of \mathbf{x} is readily obtained by Maximum-A-Posterior estimation, provided the hyperparameters $\{\gamma_i, \mathbf{B}_i\}_1^g$ and λ are estimated, which is usually carried out using Type-II maximum likelihood estimation [27].

Three iterative algorithms [15], [17] have been derived to reconstruct \mathbf{x} . We choose the Bound-Optimization based Block SBL algorithm, denoted by BSBL-BO, to show the ability of BSBL in FECG telemonitoring. Its reconstruction of non-sparse signals is achieved by setting a γ_i -pruning threshold 1 to a small value. The threshold is used to prune out small γ_i during iterations of the algorithm. A smaller value of the threshold means fewer γ_i are pruned out, and thus fewer blocks in \mathbf{x} are forced to zero blocks. Consequently, the estimated \mathbf{x} is less sparse. In our experiments we set the threshold to 0, i.e., disabling the pruning mechanism.

BSBL-BO (and other algorithms derived in [15]) has another ability, namely exploring and exploiting correlation structure in each block \mathbf{x}_i (i.e., the intra-block correlation) through estimating the matrices \mathbf{B}_i . Our experiments will show this ability makes it achieve better reconstruction performance.

Although BSBL-BO needs users to define the block partition (4), it is empirically shown [15], [17] that it is not needed to require the user-defined block partition to be the same as the true block partition. In the next two sections we will further confirm this.

III. EXPERIMENTS

Experiments were carried out using two real-world raw FECG datasets. Both datasets are widely used in the FECG community. In the first dataset, the FECG is barely visible, while in the second dataset the FECG is invisible. Thus the two datasets provide a good diversity of FECG recordings to verify the efficacy of our algorithm under various situations.

For algorithm comparison, this study chooses ten representative CS algorithms. Each of them represents a family of algorithms and has top-tier performance in its family. Thus the comparison results can be generalized to other related CS algorithms.

In the experiments, all the CS algorithms used the same sensing matrix to compress FECG recordings. Thus the energy

¹Such threshold is used in most SBL algorithms [27], not merely in the BSBL framework.

consumption of each CS algorithm was the same (reconstruction of FECG recordings is done by software in remote terminals and thus it does not cost energy of WBANs). Therefore in this section we only present reconstruction results.

In adult ECG telemonitoring or other applications, reconstruction performance is generally measured by comparing reconstructed recordings with original recordings using the mean square error (MSE) as a performance index. However, in our application reconstructing raw FECG recordings is not the final goal; the reconstructed recordings are further processed to extract a clean FECG by other advanced signal processing techniques such as BSS/ICA, sparse representation, and nonlinear filtering. Due to the infidelity of MSE for structured signals [28], it is hard to see how the final FECG extraction is affected by errors in reconstructed recordings measured by MSE. Thus, a more direct measure is to compare the extracted FECG from the reconstructed recordings with the extracted one from the original recordings. This study used BSS/ICA algorithms to extract a clean FECG from reconstructed recordings and a clean FECG from original recordings, and then calculated the correlation between the two extracted FECGs.

A. The DaISy Dataset

Figure 1 shows a segment from the DaISy dataset [29]. Two QRS complexes of MECG can be clearly seen from this segment, and two QRS complexes of FECG can be seen but not very clearly. We can clearly see that the segment is far from sparse; its every entry is non-zero. This brings a huge difficulty for existing CS algorithms to reconstruct it.

To compress the data we used a randomly generated sparse binary sensing matrix of the size 125×250 . Its each column contained 15 entries of 1s, while other entries were zero.

For the BSBL-BO algorithm, we defined its block partition according to (4) with $h_1 = \dots = h_g = 25$. Section IV will show that the algorithm is not sensitive to the block partition. The algorithm was employed in two ways. The first way was allowing it to adaptively learn and exploit intra-block correlation. The second way was preventing it from exploiting intra-block correlation, i.e. by fixing the matrices $\mathbf{B}_i, \forall i$, to identity matrices.

The results are shown in Figure 2, from which we can see that exploiting intra-block correlation allows the algorithm to reconstruct the segment with high quality. If the correlation structure is not exploited, the reconstruction quality is very poor; for example, the first QRS complex of the FECG is missing in the reconstructed segment (Figure 2 (c)).

Then we employed two groups of CS algorithms. One group was the algorithms based on the basic CS model (1), which do not exploit block structure of signals. They were CoSaMP [30], Elastic-Net [31], Basis Pursuit [32], SL0 [33], and EMBGAMP [34]. They are representative of greedy algorithms, of algorithms minimizing the combination of ℓ_1 and ℓ_2 norms, of algorithms minimizing ℓ_1 norm, of algorithms minimizing ℓ_0 norm, and of message passing algorithms, respectively. Note that the Basis Pursuit algorithm was the one used in [10] to

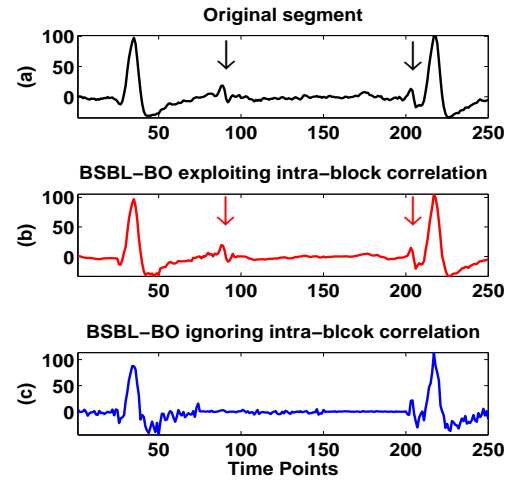


Fig. 2. Comparison of the original segment and the reconstructed segments by BSBL-BO with and without exploiting intra-block correlation. (a) The original FECG segment. (b) The reconstructed segment by BSBL-BO when exploiting intra-block correlation. (c) The reconstructed segment by BSBL-BO when not exploiting intra-block correlation. The arrows indicate QRS complexes of the fetal ECG.

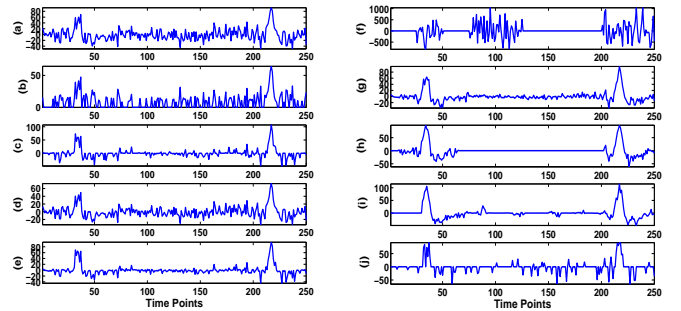


Fig. 3. Recovery results of compared algorithms. From (a) to (j), they are the results by (a) Elastic Net, (b) CoSaMP, (c) Basis Pursuit, (d) SL0, (e) EMBGAMP, (f) Block-OMP, (g) Block Basis Pursuit, (h) CluSS-MCMC, (i) StructOMP, and (j) BM-MAP-OMP, respectively.

reconstruct adult ECG recordings. Their reconstruction results are shown in Figure 3 (a)-(e) ².

The second group was the algorithms exploiting structure of signals. They were Block-OMP [21], Block Basis Pursuit [32], CluSS-MCMC [24], StructOMP [23], and BM-MAP-OMP [25]. Block-OMP and Block Basis Pursuit need *a priori* knowledge of block partition. We used the block partition in (4) with $h_1 = \dots = h_g = h$, and h varied from 2 to 50. However, neither block size yielded meaningful results. Figure 3 (f)-(g) show their results when $h = 25$. Figure 3 (h) shows the reconstruction result of CluSS-MCMC. StructOMP requires *a priori* knowledge of the sparsity (i.e. the number of nonzero entries in the segment). Since we did not know the sparsity exactly, we set the sparsity from 50 to 250. However, no sparsity value led to a good result. Figure 3 (i) shows the result with the sparsity set to 125. Figure 3 (j) shows the result

²The free parameters of these algorithms were tuned by trial and error. But no values were found to give meaningful results.

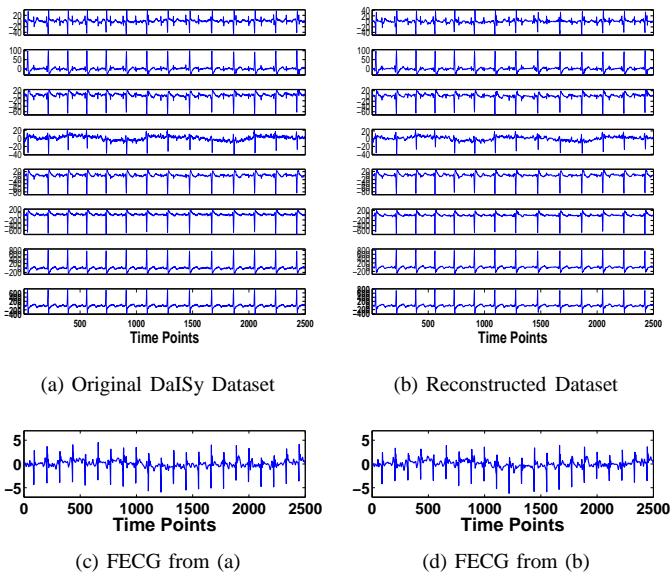


Fig. 4. (a) The original dataset. (b) The reconstructed dataset by BSBL-BO. (c) The extracted FECG from the original dataset. (d) The extracted FECG from the dataset reconstructed by BSBL-BO.

of BM-MAP-OMP.

Comparing all the results we can see only the BSBL-BO algorithm, if allowed to exploit intra-block correlation, can reconstruct the segment with satisfactory quality.

To further verify the ability of BSBL-BO, we used the same sensing matrix to compress the whole DaISy dataset, and then used BSBL-BO to reconstruct it.

Figure 4 (a) shows the whole dataset. The most obvious activity is the MEGC, which can be seen in all the recordings. The FECG is very weak, which is nearly discernible in the first five recordings. The fourth recording is dominated by a baseline wander caused by maternal respiration.

The reconstruction result by BSBL-BO is shown in Figure 4 (b). We can see all the recordings are reconstructed very well. Visually, we do not observe any distortions in the reconstructed dataset.

Admittedly, the reconstructed recordings contained small errors. Since in our application the final goal is to extract clean FECGs from reconstructed FECG recordings using advanced signal processing techniques such as BSS/ICA, we should study whether the reconstruction errors deteriorate the performance of these techniques in extracting FECGs. Here, we examined whether the errors affected the performance of BSS/ICA. We used the eigBSE algorithm, a BSS algorithm proposed in [35], to extract a clean FECG from the reconstructed recordings. The algorithm exploits quasi-periodic characteristics of FECGs. Thus, if the quasi-periodic structure of FECGs and the ICA mixing structure of the recordings are distorted, the extracted FECG will have poor quality.

Figure 4 (d) shows the extraction results. We can see the FECG is clearly extracted without losing any QRS complexes or containing residual noise/interference. For comparison, we performed the eigBSE algorithm on the original recordings to extract the FECG. The result is shown in Figure 4 (c).

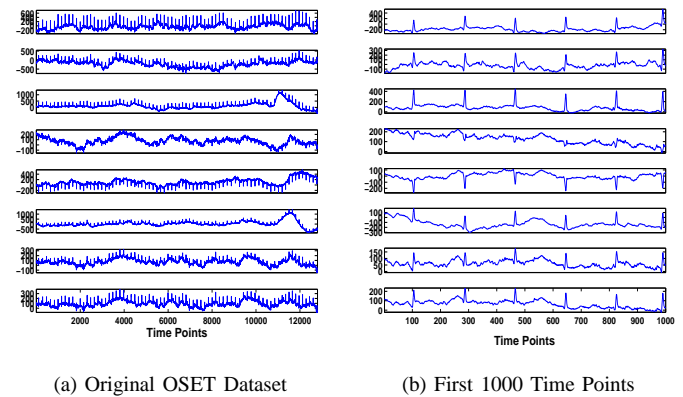


Fig. 5. The original dataset used in Section III-B. (a) The whole dataset, which contains strong baseline wander. (b) The close-up of the first 1000 time points of the recordings, where only the QRS complexes of maternal ECG can be observed. The QRS complexes of fetal ECG are not visible.

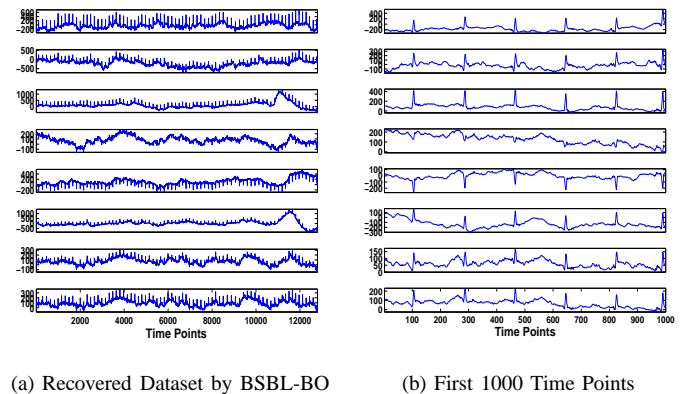


Fig. 6. The recovered dataset by BSBL-BO. (a) The recovered whole dataset. (b) The first 1000 time points of the recovered dataset. Visually, there is no difference between the original dataset and the recovered dataset.

Obviously, the two extracted FECGs are almost the same. In fact, their correlation is 0.931.

B. The OSET Dataset

The DaISy dataset is actually a clean dataset. Generally in raw FECG recordings there are many strong baseline wanders, and FECGs are very weak and are buried by noise or MEGCs. To test the ability of BSBL-BO for these worse scenarios, we used the dataset ‘signal01’ in the Open-Source Electrophysiological Toolbox (OSET) [36]. The dataset consists of eight abdominal recordings sampled at 1000 Hz. We first downsampled the dataset to 250 Hz, since in WBAN-based telemonitoring the sampling frequency rarely exceeds 500 Hz. For illustration, we selected the first 12800 time points of each downsampled recording as the dataset used in our experiment. Figure 5 (a) shows the studied dataset, where in every recording baseline wanders are significant. Figure 5 (b) shows the first 1000 time points of the recordings, where the QRS complexes of the MEGC and various kinds of noise dominate the recordings and the FECG is completely buried by them.

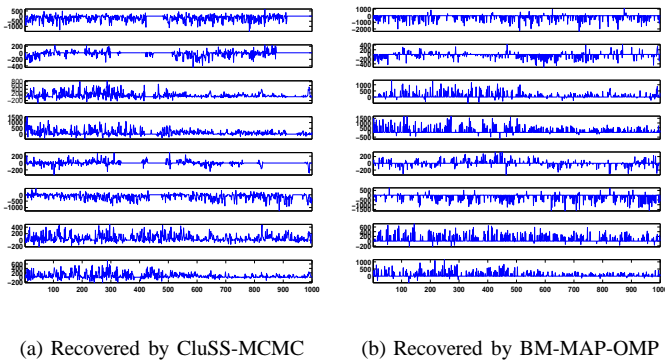


Fig. 7. The whole datasets recovered by (a) CluSS-MCMC and (b) BM-MAP-OMP, respectively.

We used another randomly generated sparse binary sensing matrix of size 256×512 with each column consisting of 12 entries of 1s with random locations, while other entries were all zero. The sensing matrix is exactly the one used in [10].

For BSBL-BO, we set the block partition $h_1 = \dots = h_{16} = 32$. The recovered dataset by BSBL-BO is shown in Figure 6 (a), and the first 1000 time points of the recovered recordings are shown in Figure 6 (b). Visually, the recovered dataset is the same as the original dataset, even the various baseline wanders are recovered well.

The ten CS algorithms used in the previous subsection were used to reconstruct the dataset. Again, they all fail. To save space, we only present the reconstruction results by CluSS-MCMC and BM-MAP-OMP in Figure 7.

Similar to the previous subsection, we used BSS/ICA to extract the FECG and then compared it to the one extracted from the original dataset. Here we used another ICA algorithm, the FastICA algorithm [37].

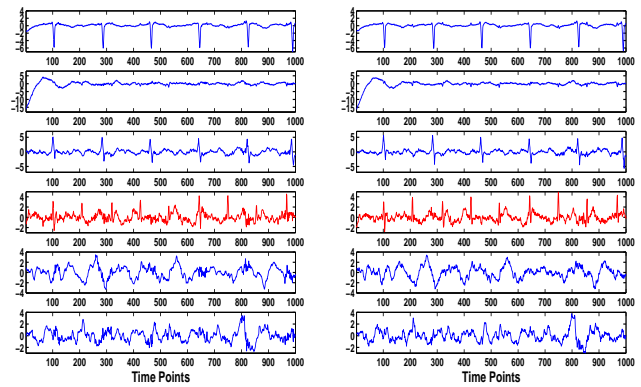
First, the reconstructed dataset was band-passed from 1.75 Hz to 100 Hz (note that in telemonitoring, it is done in the reconstruction stage in remote terminals). Then, FastICA was performed in the ‘deflation’ mode. Six independent components (ICs) with significant non-Gaussianity were extracted, as shown in Figure 8 (a), where the fourth IC is the FECG.

Then FastICA was performed on the original dataset. The ICs are shown in Figure 8 (b). Comparing Figure 8 (a) with Figure 8 (b) we can see the distortion is very small, which obviously does not affect clinical diagnosis.

To reconstruct non-sparse signals, a conventional approach in the CS field is to adopt the model (2), namely, first reconstructing θ using the received data y and the known matrix $\Phi\Psi$, and then calculating x by $x = \Psi\theta$. To test whether this approach is helpful for existing CS algorithms to reconstruct raw FECG recordings, in the following we repeated the experiment in Section III-B using the previous ten CS algorithms and adopting the approach.

Since it is shown [13] that Daubechies 4 wavelet can yield the sparsest representation of ECG, we set the dictionary matrix Ψ to be the inverse of the Daubechies 4 wavelet transform matrix. The sensing matrix was the one used in Section III-B.

Unfortunately, all these CS algorithms fail again. The FECG



(a) ICA of the Reconstructed Dataset (b) ICA of the Original Dataset

Fig. 8. Comparison of the ICA decomposition of the original dataset and the recovered dataset by BSBL-BO. (a) The ICs of the recovered dataset. (b) The ICs of the original dataset. The fourth ICs in (a) and (b) are the extracted FECGs from the reconstructed dataset and the original dataset, respectively.

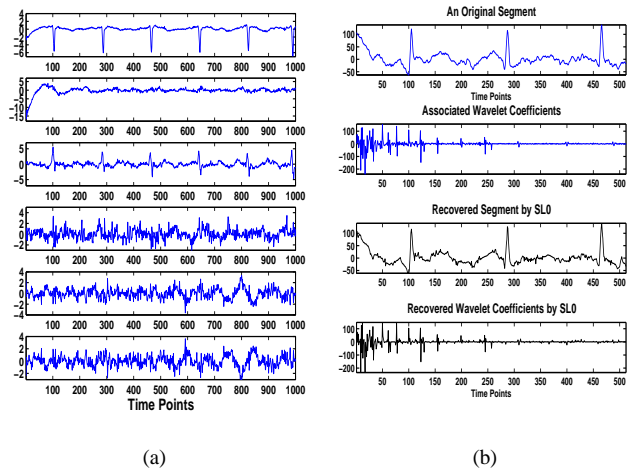


Fig. 9. Reconstruction result by SL0 with the aid of the wavelet transform. (a) The ICs of the recovered dataset by SL0. (b) From top to bottom are a segment of the original dataset, the associated wavelet coefficients, the recovered segment by SL0, and the recovered wavelet coefficients by SL0.

cannot be extracted from the dataset reconstructed by any of these CS algorithms. Figure 9 (a) shows the ICs extracted from the dataset reconstructed by SL0 based on the wavelet transform. The FECG has not been extracted.

Therefore, using the wavelet transform is still not helpful for these CS algorithms. The reason is that to ensure the FECG can be extracted by ICA with high fidelity, the ICA mixing structure should be maintained well in the reconstructed dataset. This requires that wavelet coefficients with small amplitudes in addition to those with large amplitudes are all recovered well. However, for a raw FECG recording the wavelet coefficients with small amplitudes are overwhelmed. To recover these coefficients is still difficult for most CS algorithms.

As an example, the top two panels in Figure 9 (b) show a segment of a raw recording and its wavelet coefficients, respectively. The bottom two panels in Figure 9 (b) show the recovered segment and the recovered wavelet coefficients

by SL0, respectively. We can see the coefficients with large amplitudes are recovered well. It is the failure to recover the coefficients with small amplitudes that results in the failure of extracting the FECG.

IV. ISSUES ON THE PERFORMANCE OF BSBL-BO

This section explores how the performance of BSBL-BO is affected by various experimental factors, such as the signal-to-noise-ratio, user-defined block partition, compression ratio, and sensing matrices.

A. Effects of Signal-to-Interference-and-Noise Ratio

We have tested BSBL-BO's performance using two typical datasets. The two datasets contain MEGC and noise with certain strength. It is natural to ask whether BSBL-BO can be used for other datasets containing MEGC and noise with different strength. This question is very important, since different fetus positions, different pregnancy weeks, and random muscle movements can result in dramatic changes in correlation structure of raw recordings, while BSBL-BO exploits the correlation structure for improved performance.

Therefore, we carried out Monte Carlo simulations with different strength of FECGs, MEGCs, and other noise, as in [38]. The raw multichannel recordings were modeled as the summation of a multichannel FECG, a multichannel MEGC, and multichannel noise. The multichannel MEGC was generated by a three-dimensional dipole which projects cardiac potentials to eight sensors. The multichannel FECG was generated in the same way with half period of the MEGC. The angle between the two dipoles generating FECG potential and MEGC potential was 41° . The noise was randomly selected real-world baseline wanders, muscle artifacts, and electrode movement artifacts from the Noise Stress Test Database (NSTDB) [39]. Details on the simulation design can be found in [38, Sec. V.A]. The generated raw recordings were downsampled to 250 Hz. Each recording finally contained 7680 time points.

As in [38], the ratio of the power of the multichannel FECG to the power of the multichannel MEGC was defined as the signal-to-interference ratio (SIR). The ratio of the power of the multichannel FECG to the power of the multichannel noise was defined as the signal-to-noise ratio (SNR). And the ratio of the power of the FECG to the summarized power of the MEGC and the noise was defined as the signal-to-Interference-and-Noise ratio (SINR). In the simulation, the strength of the FECG, the MEGC and the noise were adjusted so that $\text{SNR} = \text{SIR} + 10\text{dB}$, and SINR was swept in the range of -35dB to -15dB . Note that the SINR range was intentionally made more challenging, since for most raw recordings the SINR varies only from -5dB to -25dB [40]. For each value of the SINR, the simulation was repeated 20 times, each time with different signal and noise.

The sensing matrix and the block partition of BSBL-BO were the same as in Section III-B. The result presented in Figure 10 clearly shows the high recovery quality of BSBL-BO even in the worst noisy scenarios. Figure 11 shows a generated dataset when $\text{SINR}=-35\text{dB}$, and the extracted FECGs from the generated dataset and from the recovered dataset. We can see

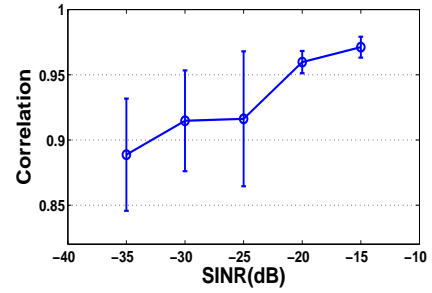


Fig. 10. The correlation (averaged over 20 trials) between the extracted FECG from the original generated dataset and the one from the recovered dataset at different SINR. The error bar gives the standard variance.

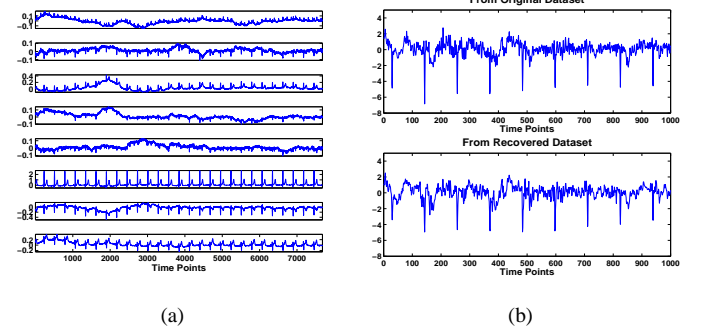


Fig. 11. A synthesized dataset and the extraction result at $\text{SINR}=-35\text{dB}$. (a) The synthesized dataset. (b) The comparison between the extracted FECG from the synthesized dataset and the one from the corresponding recovered dataset (only their first 1000 time points are shown).

the noise is very strong, but the extracted FECG from the recovered dataset still maintains high fidelity.

B. Effects of the Block Partition

In all the previous experiments we used certain block partitions. Another question is, "Is the performance of BSBL-BO sensitive to the block partition?" To examine this, the following experiment was carried out.

We used the dataset and the sensing matrix used in Section III-B. The block partition was designed as follows: the location of the first entry of each block was $1, 1+h, 1+2h, \dots$, where the block size h ranged from 4 to 80.

The results are shown in Fig.12, from which we can see that the extraction quality is almost the same over a broad range of h . The reason that $h = 40$ and $h = 44$ lead to low quality is unknown. But note that the result is based on the use of a single sensing matrix. We find other sensing matrices (the number of non-zero entries in each column is the same but their locations are different) lead to good quality at $h = 40$ and $h = 44$. Based on experiments using ten different sensing matrices, $12 \leq h \leq 36$ always lead to satisfactory results.

C. Effect of Compression Ratio

Next, we investigate the effect of compression ratio (CR) on the quality of extracted FECGs from reconstructed recordings. The compression ratio is defined as

$$CR = \frac{N - M}{N} \times 100 \quad (6)$$

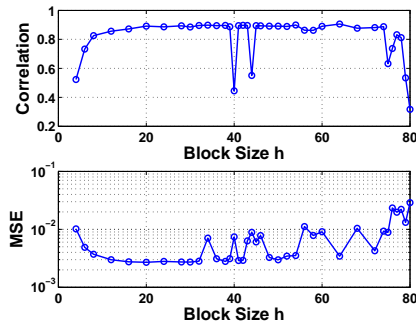


Fig. 12. Effect of the block size h on the final extraction quality of FECGs, measured by the correlation between the extracted FECG from the reconstructed dataset and the extracted one from the original dataset. The block size h ranged from 4 to 80.

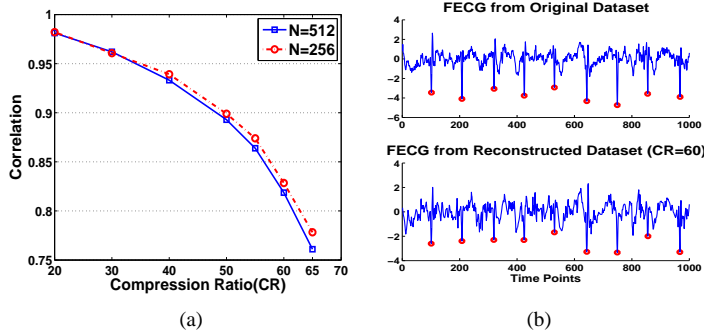


Fig. 13. Experiment results in Section IV-C. (a) The effect of the compression ratio on the quality of extracted FECGs from reconstructed dataset (measured by correlation) when $N = 512$ and $N = 256$. (b) The extracted FECG from the original dataset and from the reconstructed dataset when $CR=60$ and $N = 512$ (only first 1000 time points are shown). Red circles indicate the detected peaks of R-waves in both FECGs.

where N is the length of the original signal and M is the length of the compressed signal. The used sparse binary sensing matrix had the size of $M \times N$, where N was fixed to 512, while M varied so that CR ranged from 20 to 65. Regardless of the size, its each column contained 12 entries of 1s. For each value of M , we repeated the experiment 20 times, and in each repeated experiment the sensing matrix was randomly generated. The dataset and the block partition for BSBL-BO were the same as in Section III-B.

The averaged results for each CR are shown in Figure 13 (a). We find that when $CR \leq 60$, the quality of extracted FECGs is satisfactory and can be used for clinical diagnosis. For example, Figure 13 (b) shows the extracted FECG from a reconstructed dataset when $CR=60$. Compared to the FECG extracted from the original dataset, the FECG from the reconstructed dataset does not have significant distortion. Especially, when using the 'PeakDetection' program in the OSET toolbox to detect peaks of the R-waves in both extracted FECGs, the results are the same, as shown in Figure 13 (b).

We repeated the experiment using a smaller sparse binary matrix with $N = 256$. Each column also contained 12 entries of 1s. The block size in the block partition for BSBL-BO did not change. The result (Figure 13 (a)) shows that the quality of extracted FECGs is slightly better than the case of $N = 512$.

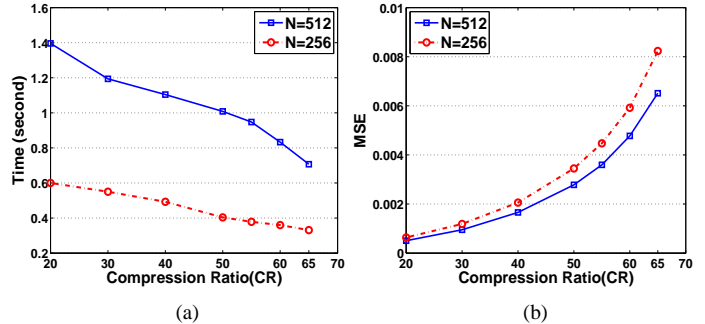


Fig. 14. (a) Comparison of averaged time in reconstructing a segment of 512 time points from the dataset shown in Figure 5 when using two sensing matrices. Note that it took 2.048 seconds to collect a segment of 512 time points. But the algorithm took less than 1.4 seconds to recover the segment in a laptop with 2.8G CUP and 6G RAM if using the big sensing matrix, or took less than 0.6 seconds if using the small sensing matrix. (b) Comparison of MSE in reconstructing the dataset when using the two sensing matrices.

Note that a significant advantage of using a smaller sensing matrix is that the reconstruction speeds up. Figure 14 (a) compares the averaged time in reconstructing a segment of 512 time points when using the two sensing matrices at different CRs. Clearly, using a small sensing matrix speeds up the reconstruction, making it possible to build a near real-time telemonitoring system.

It is worth noting that when fixing CR, using smaller sensing matrices generally results in higher MSE measured on reconstructed recordings, as shown in Figure 14 (b). But this does not mean the quality of extracted FECGs is poorer accordingly, as shown in Figure 13 (a). The reason is that MSE is not a good measure for structured signals.

D. Study on the Number of Non-zero Entries in Each Column of the Sensing Matrix

In most of the experiments we used a 256×512 sensing matrix, whose each column contained 12 entries of 1s. This number of non-zero entries in each column was chosen by Mamaghanian et al according to their study [10] using an ordinary ℓ_1 CS algorithm. To study how the number of non-zero entries in each column affects the performance of BSBL-BO, we carried out a similar experiment as in [10].

The sparse binary sensing matrix had the size of 256×512 . Each column contained d entries of 1s, where d varied from 2 to 14. The experiment was repeated 20 times for each value of d . In each repeated experiment, the locations of the non-zero entries were randomly chosen (but the generated sensing matrix was always full-rank). The dataset and the block partition were the same as in Section III-B.

Figure 15 (a) shows the correlation of extracted FECGs from reconstructed datasets to the extracted FECG from the original dataset. Figure 15 (b) shows the quality of reconstructed datasets measured in MSE. Both figures clearly show that the results are not affected by d . This is totally different from the result in [10] using an ordinary ℓ_1 CS algorithm, suggesting another advantage of BSBL-BO.

This advantage of BSBL-BO is very important for energy saving. When the size of a sparse binary sensing matrix is

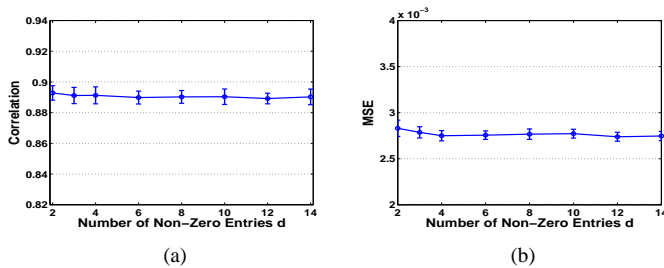


Fig. 15. Relation between reconstruction results and the number of entries of 1s in each column of the sensing matrix. (a) The correlation between the extracted FECGs from the reconstructed dataset and the FECG from the original dataset. (b) MSE of the reconstructed dataset. The error bar gives the standard variance.

fixed, the energy consumption is directly related to d . Using a sensing matrix with $d = 2$ can cost only about 1/6 of the energy in compressing data, compared to using a sensing matrix with the same size but $d = 12$.

V. DISCUSSIONS

A. The Block Partition in the BSBL Framework

The reconstruction of a raw FECG recording can be cast as a block sparse model with unknown block partition and unknown signal noise in a noiseless environment. To exploit the unknown block structure, our algorithm is based on a very simple and even counter-intuitive strategy. That is, *the user-defined block partition can be rather random, which is not required to be the same as the true block structure of the FECG recording*. This strategy is completely different from the strategies used by other CS algorithms to deal with unknown block structure, which try to find the true block structure as accurate as possible [24], [25]. In fact, in the BSBL framework, the block partition is a regularization for better learning the covariance matrix of \mathbf{x} in a high-dimensional space. Theoretical explanation to our empirical strategy for the BSBL framework is an important topic in the future.

B. Reconstruction of Non-Sparse Signals

Most raw physiological signals are not sparse, especially when contaminated by noise from baseline wanders and muscle movements. Reconstructing these signals is essentially reconstructing non-sparse signals. To reconstructing these non-sparse signals, there are two often-used strategies.

One is using thresholding [14] to set those entries with small amplitudes to zero. However, these thresholding methods cannot be used for FECG recordings. As we have seen, the amplitudes of FECGs are very small and even invisible, and thus it is difficult or even impossible to choose an optimal threshold value. What's worse is that the thresholding methods can destroy interdependence structure among multichannel recordings, such as the ICA mixing structure among FECG raw recordings.

Another strategy widely used by CS algorithms to reconstruct non-sparse signals is based on transform domains, as mathematically expressed in (2). The success of this strategy depends on whether the representation coefficients θ are

sparse. Unfortunately, for raw FECG recordings and many other physiological signals, the representation coefficients θ are still not sparse enough; although coefficients with large amplitudes are few, coefficients with small amplitudes are numerous. When reconstructed signals are going to be further processed by other complicated signal processing/machine learning techniques, reconstructing these coefficients with small amplitudes is very important. As shown in this work, failure to reconstruct these coefficients results in the failure of ICA to extract FECGs.

The BSBL-BO algorithm, unlike existing algorithms, directly reconstructs non-sparse signals without resorting to the above two strategies. Clearly, exploiting block structure and intra-block correlation plays a crucial role in the reconstruction. The reconstruction with high fidelity allows further signal processing or pattern recognition for clinical diagnosis.

C. Ultra-Low Compression Realized by the BSBL Framework

This work focuses on algorithms for wireless FECG tele-monitoring. It does not involve the analysis of energy consumption, especially the comparison between BSBL-BO with wavelet compression. However, this issue actually has been addressed in the work by Mamaghanian et al. [10]. According to their 'digital CS' paradigm, if two CS algorithms use the same sensing matrix, their energy consumption is the same. Since in most experiments we used the same sparse binary matrix as theirs (12 entries of 1s in each column of Φ), their analysis on the energy consumption and their comparison to wavelet compression are applicable to BSBL-BO.

But BSBL-BO can further reduce the energy consumption while maintaining the same reconstruction performance. In Section IV-D we have shown that BSBL-BO has the same performance regardless of the value of d , i.e., the number of entries of 1s in each column of Φ . Thus, we can use a sparse binary matrix with $d = 2$ to save more energy. For example, when compressing a signal of 512 time points to 256 time points, using a sparse binary sensing matrix with $d = 2$ only needs about 768 additions, while using a sparse binary sensing matrix with $d = 12$ requires about 5888 additions, and using the Daubechies 4 Wavelet to compress the signal requires 11784 multiplications and 11272 additions (in addition, its seeking large coefficients also cost a lot of energy). Thus, using the sparse binary matrix with $d = 2$ can greatly reduce code execution on CPU, and thus reduce energy consumption.

It should be noted that only BSBL-BO (and other algorithms derived from the BSBL framework) can use such a sparse binary matrix to compress signals. Our experiments on adult ECGs³ show that other CS algorithms fail to reconstruct or have seriously degraded reconstruction quality when using the sparse binary matrix to compress adult ECGs. In [10] it is also shown that the basis pursuit algorithm is very sensitive to d ; when d decreases from 12 to 2, the reconstruction performance measured by output SNR decreases from 20 dB to 7 dB (when the sensing matrix has the size of 256×512).

³Since the compared ten CS algorithms fail to reconstruct FECG recordings, we used adult ECGs without noise to carry out the experiments. Due to space limit the results are omitted here.

This significant advantage implies that BSBL-BO, compared to many existing data compression techniques, consumes ultra-low energy in the data compression stage.

VI. CONCLUSIONS

Fetal ECG telemonitoring via wireless body-area networks with low-energy constraint is a challenge for CS algorithms. This work showed that the block sparse Bayesian learning framework [15] can be successfully employed in this task. Its success relies on two unique abilities; one is the ability to reconstruct non-sparse structured signals, and the other is the ability to explore and exploit correlation structure of signals to improve performance. Although the focus is the wireless FECG telemonitoring, the proposed framework and associated algorithms can be used to many other e-Health applications, such as telemonitoring of adult ECG [10], [13], wireless electroencephalogram [41], and electromyography [14].

REFERENCES

- [1] J. Smith Jr, "Fetal health assessment using prenatal diagnostic techniques," *Current Opinion in Obstetrics and Gynecology*, vol. 20, no. 2, p. 152, 2008.
- [2] M. Hasan, M. Reaz, M. Ibrahimy, M. Hussain, and J. Uddin, "Detection and processing techniques of FECG signal for fetal monitoring," *Biological procedures online*, vol. 11, no. 1, pp. 263–295, 2009.
- [3] R. Sameni, M. Shamsollahi, C. Jutten, and G. Clifford, "A nonlinear bayesian filtering framework for ECG denoising," *IEEE Transactions on Biomedical Engineering*, vol. 54, no. 12, pp. 2172–2185, 2007.
- [4] P. Addison, "Wavelet transforms and the ECG: a review," *Physiological measurement*, vol. 26, p. R155, 2005.
- [5] L. De Lathauwer, B. De Moor, and J. Vandewalle, "Fetal electrocardiogram extraction by blind source subspace separation," *IEEE Transactions on Biomedical Engineering*, vol. 47, no. 5, pp. 567–572, 2000.
- [6] R. Sameni and G. Clifford, "A review of fetal ECG signal processing; issues and promising directions," *The open pacing, electrophysiology & therapy journal*, vol. 3, p. 4, 2010.
- [7] *Special Issue on Cyber-Physical Systems, Proceedings of the IEEE*, 2012, vol. 100, no. 1.
- [8] H. Cao, V. Leung, C. Chow, and H. Chan, "Enabling technologies for wireless body area networks: A survey and outlook," *IEEE Communications Magazine*, vol. 47, no. 12, pp. 84–93, 2009.
- [9] A. Milenkovic, C. Otto, and E. Jovanov, "Wireless sensor networks for personal health monitoring: Issues and an implementation," *Computer communications*, vol. 29, no. 13–14, pp. 2521–2533, 2006.
- [10] H. Mamaghanian, N. Khaled, D. Atienza, and P. Vandergheynst, "Compressed sensing for real-time energy-efficient ECG compression on wireless body sensor nodes," *IEEE Transactions on Biomedical Engineering*, vol. 58, no. 9, pp. 2456–2466, 2011.
- [11] D. Donoho, "Compressed sensing," *Information Theory, IEEE Transactions on*, vol. 52, no. 4, pp. 1289–1306, 2006.
- [12] E. Candes, J. Romberg, and T. Tao, "Stable signal recovery from incomplete and inaccurate measurements," *Communications on pure and applied mathematics*, vol. 59, no. 8, pp. 1207–1223, 2006.
- [13] C. Eduardo, P. Octavian Adrian, S. Pedro, et al., "Implementation of compressed sensing in telecardiology sensor networks," *International Journal of Telemedicine and Applications*, vol. 2010, 2010.
- [14] A. M. Dixon, E. G. Allstot, D. Gangopadhyay, and D. J. Allstot, "Compressed sensing system considerations for ECG and EMG wireless biosensors," *IEEE Trans. on Biomedical Circuits and Systems*, vol. 6, no. 2, pp. 156–166, 2012.
- [15] Z. Zhang and B. Rao, "Extension of SBL algorithms for the recovery of block sparse signals with intra-block correlation," *IEEE Trans. on Signal Processing (submitted)*, 2012. [Online]. Available: arXiv:1201.0862
- [16] —, "Sparse signal recovery with temporally correlated source vectors using sparse Bayesian learning," *IEEE Journal of Selected Topics in Signal Processing*, vol. 5, no. 5, pp. 912–926, 2011.
- [17] —, "Recovery of block sparse signals using the framework of block sparse Bayesian learning," in *2012 IEEE International Conference on Acoustics, Speech and Signal Processing (ICASSP)*, 2012.
- [18] —, "Exploiting correlation in sparse signal recovery problems: Multiple measurement vectors, block sparsity, and time-varying sparsity," in *ICML 2011 Workshop on Structured Sparsity: Learning and Inference*, 2011. [Online]. Available: <http://arxiv.org/pdf/1105.0725>
- [19] J. Wan, Z. Zhang, J. Yan, T. Li, B. D. Rao, and et al, "Sparse Bayesian multi-task learning for predicting cognitive outcomes from neuroimaging measures in Alzheimers disease," in *CVPR 2012*.
- [20] E. Arias-Castro and Y. Eldar, "Noise folding in compressed sensing," *IEEE Signal Processing Letters*, vol. 18, no. 4, pp. 478 – 481, 2011.
- [21] Y. C. Eldar, P. Kuppinger, and H. Bolcskei, "Block-sparse signals: uncertainty relations and efficient recovery," *IEEE Trans. on Signal Processing*, vol. 58, no. 6, pp. 3042–3054, 2010.
- [22] R. G. Baraniuk, V. Cevher, M. F. Duarte, and C. Hegde, "Model-based compressive sensing," *IEEE Trans. on Information Theory*, vol. 56, no. 4, pp. 1982–2001, 2010.
- [23] J. Huang, T. Zhang, and D. Metaxas, "Learning with structured sparsity," in *Proceedings of the 26th Annual International Conference on Machine Learning*, 2009, pp. 417–424.
- [24] L. Yu, H. Sun, J. P. Barbot, and G. Zheng, "Bayesian compressive sensing for cluster structured sparse signals," *Signal Processing*, vol. 92, no. 1, pp. 259–269, 2012.
- [25] T. Peleg, Y. Eldar, and M. Elad, "Exploiting statistical dependencies in sparse representations for signal recovery," *IEEE Trans. on Signal Processing*, vol. 60, no. 5, pp. 2286–2303, 2012.
- [26] Z. Zhang and B. Rao, "Clarify some issues on the sparse Bayesian learning for sparse signal recovery," *Technical Report, University of California, San Diego*, Sep. 2011. [Online]. Available: <http://dsp.ucsd.edu/~zhilin/papers/clarify.pdf>
- [27] M. E. Tipping, "Sparse Bayesian learning and the relevance vector machine," *J. of Mach. Learn. Res.*, vol. 1, pp. 211–244, 2001.
- [28] Z. Wang and A. Bovik, "Mean squared error: Love it or leave it? a new look at signal fidelity measures," *IEEE Signal Processing Magazine*, vol. 26, no. 1, pp. 98–117, 2009.
- [29] B. D. Moor, "DaISy: Database for the identification of systems," November 2011. [Online]. Available: <http://www.esat.kuleuven.ac.be/sista/daisy>
- [30] D. Needell and J. A. Tropp, "CoSaMP: Iterative signal recovery from incomplete and inaccurate samples," *Applied and Computational Harmonic Analysis*, vol. 26, no. 3, pp. 301–321, 2009.
- [31] H. Zou and T. Hastie, "Regularization and variable selection via the elastic net," *Journal of the Royal Statistical Society: Series B (Statistical Methodology)*, vol. 67, no. 2, pp. 301–320, 2005.
- [32] E. Van Den Berg and M. Friedlander, "Probing the pareto frontier for basis pursuit solutions," *SIAM Journal on Scientific Computing*, vol. 31, no. 2, pp. 890–912, 2008.
- [33] H. Mohimani, M. Babaie-Zadeh, and C. Jutten, "A fast approach for overcomplete sparse decomposition based on smoothed l0 norm," *IEEE Trans. on Signal Processing*, vol. 57, no. 1, pp. 289–301, 2009.
- [34] J. Vila and P. Schniter, "Expectation-maximization bernoulli-gaussian approximate message passing," in *Proc. Asilomar Conf. on Signals, Systems, and Computers*, 2011.
- [35] Z.-L. Zhang and Z. Yi, "Robust extraction of specific signals with temporal structure," *Neurocomputing*, vol. 69, no. 7–9, pp. 888–893, 2006.
- [36] R. Sameni, "OSET: The open-source electrophysiological toolbox," January 2012. [Online]. Available: <http://www.oset.ir/>
- [37] A. Hyvarinen, "Fast and robust fixed-point algorithms for independent component analysis," *IEEE Transactions on Neural Networks*, vol. 10, no. 3, pp. 626–634, 1999.
- [38] R. Sameni, C. Jutten, and M. Shamsollahi, "A deflation procedure for subspace decomposition," *IEEE Transactions on Signal Processing*, vol. 58, no. 4, pp. 2363–2374, 2010.
- [39] G. Moody, W. Muldrow, and R. Mark, "The MIT-BIH noise stress test database." [Online]. Available: <http://www.physionet.org/physiobank/database/nstdb>
- [40] R. Shepovalnikov, A. Nemirko, A. Kalinichenko, and V. Abramchenko, "Investigation of time, amplitude, and frequency parameters of a direct fetal ECG signal during labor and delivery," *Pattern Recognition and Image Analysis*, vol. 16, no. 1, pp. 74–76, 2006.
- [41] C. Lin, L. Ko, J. Chiou, J. Duann, R. Huang, S. Liang, T. Chiu, and T. Jung, "Noninvasive neural prostheses using mobile and wireless EEG," *Proceedings of the IEEE*, vol. 96, no. 7, pp. 1167–1183, 2008.